Available online at www.sciencedirect.com
ScienceDirect
Journal of Power Sources 179 (2008) 640–648
JOURNAL OF POWER SOURCES
www.elsevier.com/locate/jpowsour

# Initialization of a methane-fueled single-chamber solid-oxide fuel cell with NiO + SDC anode and BSCF + SDC cathode

Chunming Zhang [a], Yao Zheng [a], Ran Ran [a], Zongping Shao [a,*], Wanqin Jin [a], Nanping Xu [a], Jeongmin Ahn [b]

[a] *State Key Laboratory of Materials-Oriented Chemical Engineering, College of Chemistry & Chemical Engineering, Nanjing University of Technology, No. 5 Xin Mofan Road, Nanjing, JiangSu 210009, PR China*
[b] *School of Mechanical and Materials Engineering, Washington State University, Sloan 217, Pullman, WA 99164-2920, USA*

Received 11 December 2007; received in revised form 10 January 2008; accepted 10 January 2008
Available online 21 January 2008

**Abstract**

The initialization of an anode-supported single-chamber solid-oxide fuel cell, with $NiO + Sm_{0.2}Ce_{0.8}O_{1.9}$ anode and $Ba_{0.5}Sr_{0.5}Co_{0.8}Fe_{0.2}O_{3-\delta} + Sm_{0.2}Ce_{0.8}O_{1.9}$ cathode, was investigated. The initialization process had significant impact on the observed performance of the fuel cell. The in situ reduction of the anode by a methane–air mixture failed. Although pure methane did reduce the nickel oxide, it also resulted in severe carbon coking over the anode and serious distortion of the fuel cell. In situ initialization by hydrogen led to simultaneous reduction of both the anode and cathode; however, the cell still delivered a maximum power density of ~350 mW cm$^{-2}$, attributed to the re-formation of the BSCF phase under the methane–air atmosphere at high temperatures. The ex situ reduction method appeared to be the most promising. The activated fuel cell showed a peak power density of ~570 mW cm$^{-2}$ at a furnace temperature of 600 °C, with the main polarization resistance contributed from the electrolyte.


*Keywords:* Single chamber; Solid-oxide fuel cell (SOFC); $Ba_{0.5}Sr_{0.5}Co_{0.8}Fe_{0.2}O_{3-\delta}$; Methane

## 1. Introduction

Fuel cell technology is reputed for its high-energy efficiency, favorable power density and extremely low emissions [1,2]. In association with the hydrogen economy, it has been strongly promoted during the past decades by the governments of most of the world's leading industrialized nations. Amongst the many types of fuel cells, the Solid-oxide fuel cell (SOFC) is of particular interest for its high fuel flexibility. In addition to hydrogen, other more stable chemicals, such as carbon monoxide, hydrocarbons (methane, ethane and propane) and alcohols (methanol, ethanol) can also serve as potential fuels [3–5].

A typical SOFC is composed of a porous anode and cathode that are sandwiched by a dense electrolyte. In a normal configuration, sealants are applied in order to separate the fuel cell into the fuel and oxidant chambers. The function of the dense solid-oxide electrolyte and sealant is to avoid the direct mixing of the fuel and oxidant, otherwise resulting in a decrease in fuel efficiency due to the non-electrochemical gas-phase combustion of the fuel. Currently, a single-chamber solid-oxide fuel cell (SC-SOFC) configuration has been proposed, in which the anode and cathode are exposed to a gas mixture of combined fuel and oxidant (air) [6–10]. This configuration, characterized by eliminating sealing, greatly improves the fuel cell integrity. This is due to the fact that the thermal cycling stress, which is due to the mismatch of thermal expansion between components in the fuel cell, is significantly reduced. Therefore, the SC-SOFC allows for rapid start up and shut down, which is of particular importance for small-scale power generation [11,12]. Furthermore, the anode and cathode can be deposited onto the same electrolyte surface, which allows for a versatile cell design [13,14].

The basic operating principle of a SC-SOFC surrounds the different catalytic selectivity of the electrodes towards the fuel–oxidant mixture [15,16]. Ideally, the cathode is active

* Corresponding author. Tel.: +86 25 83587722; fax: +86 25 83365813.
*E-mail address:* shaozp@njut.edu.cn (Z. Shao).

0378-7753/$ – see front matter © 2008 Elsevier B.V. All rights reserved.
doi:10.1016/j.jpowsour.2008.01.030

only for the electro-catalytic reduction of oxygen, while the anode has high activity for partial oxidation of fuel to syngas ($CO + H_2$) and also for the electro-catalytic oxidation of syngas to water and carbon dioxide. The non-ideal performance of the electrodes would create a mixed potential, which decreases both open circuit voltage (OCV) and fuel efficiency.

Recently, methane-fueled SC-SOFCs have received a lot of attention [17–25]. Shao and co-workers reported $Ba_{0.5}Sr_{0.5}Co_{0.8}Fe_{0.2}O_{3-\delta} + Sm_{0.15}Ce_{0.85}O_{1.925}$ (BSCF + SDC) to be an efficient cathode material for methane or propane-fueled SC-SOFCs [26,27]. In addition, the typical SOFC anode component, nickel, was found to be a good catalyst for the partial oxidation of methane to syngas at intermediate temperatures. Under optimized conditions, a peak power density as high as 760 mW $cm^{-2}$ was reported for a thin-film electrolyte fuel cell with a Ni + SDC anode and a BSCF + SDC (70:30 wt.%) cathode operated on a methane–oxygen–helium stream [28].

The actual electro-catalyst in the SOFC anode is metal nickel; however, there are two obvious advantages of applying NiO instead of metal nickel as the raw material for the fuel cell fabrication. First, such fabrication can be performed in air, which greatly reduces the processing cost; secondly, the reduction of nickel oxide to nickel can introduce pores into the anode layer, which facilitates the gas diffusion. The SOFC initialization, which mainly involves the reduction of nickel oxide to nickel in the anode, then becomes an important step of the fuel cell application. In situ reduction is usually adopted for dual-chamber SOFCs since the cathode environment is independent from the anode if the sealing is perfect. The situation for the SC-SOFC is much more complicated due to the fact that the anode and cathode are exposed to the same atmosphere. Especially for the cobalt-based cathode, the proper initialization procedure is critical in order to ensure high fuel cell performance.

In this paper, the initialization of a methane-fueled SC-SOFC with a NiO + SDC anode and a BSCF + SDC cathode will be systematically investigated. The different initialization processes were found to have significant impact on the SC-SOFC performance.

## 2. Experimental

### 2.1. Fuel cell fabrication

The fuel cell employed in this study was in an anode-supported thin-film electrolyte configuration with a NiO + SDC anode (~600 μm), SDC electrolyte (20–30 μm) and a BSCF + SDC (70:30 wt.%) cathode (10–20 μm). All of the fuel cell materials, except for the NiO (Chengdu Shudu Nanomaterials Technology Development Co. Ltd.), were synthesized using the standard combined EDTA-citrate complexing sol–gel process, with metal nitrates (analytical reagents) applied as the raw materials for the metal sources. Please refer to previous publications for information regarding the detailed procedure of the preparation process [29,30]. A dry-pressing/sintering method was adopted in order to fabricate the anode-supported SDC bi-

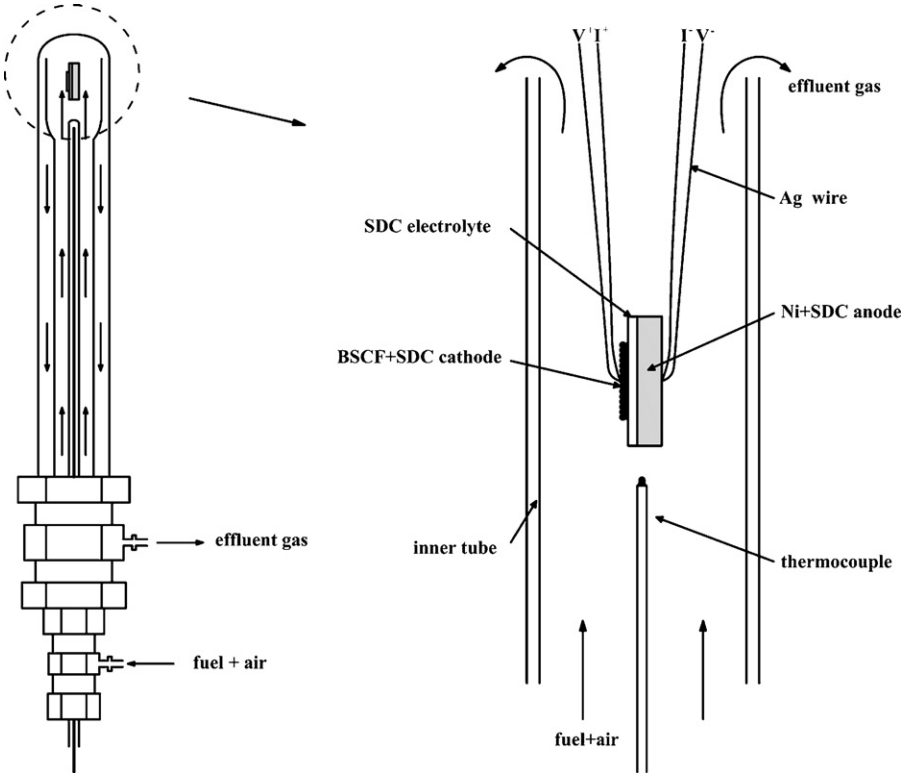


Fig. 1. Schematic of the single-chamber reactor.

layer pellets. These green dual-layer pellets resulting from dry pressing were fired at 1450 °C for 5 h in air, in order to achieve the densification of the electrolyte layer and the firm connection between the dual layers. The cathode powders (BSCF + SDC) were first dispersed in a pre-mixed solution of glycerol, ethylene glycol and isopropyl alcohol to form a colloidal suspension through high-energy ball milling (Fritsch, Pulverisettle 6), at the rotational speed of 400 rpm for 0.5 h. The resulting slurry was painted on the electrolyte surface of the fresh or pre-reduced dual-layer membranes, then calcined at 950 °C for 2 h in air (or under flowing nitrogen atmosphere for the cells with pre-reduced anode) to obtain three-layered single cells. The resulting coin-shaped cathode had an effective geometric surface area of 0.48 $cm^2$.

### 2.2. Fuel cell performance test

Four types of operational modes were exploited: (1) in situ reduction of the anode by methane–air mixed gas; (2) in situ activation by pure methane; (3) in situ initialization by hydrogen; (4) pre-reduction of the anode before the deposition of the cathode layer. The single-chamber reactor, applied for the fuel cell performance test, is schematically shown in Fig. 1. It is comprised of two quartz tubes. The outer tube has an inner diameter of ∼18 mm, while the inner tube has an outer diameter of ∼10 mm. The top of the inner tube was enlarged to a size of ∼14 mm (inner diameter) for holding the fuel cell. An electrical furnace was utilized for heating the fuel cell. Methane and air were controlled through using mass flow controllers. The methane or methane–air mixture was then introduced to the reactor through the small tube. The effluent gas escaped from the reactor through the gap between the inner and outer tube. Once the fuel cell was initialized, the methane–air gas mixture was turned on. *I–V* polarization curves were then collected using a Keithley 2420 source meter based on the four-terminal configuration. Ag paste, instead of platinum paste, was adopted as the current collector since Pt is catalytically active for methane partial oxidation.

### 2.3. Catalytic activity test

The catalytic activity of the anode or cathode materials for the methane–air conversion was evaluated in a flow-through fixed bed reactor, which is composed of a quartz tube with an inner diameter of ∼8 mm. About 0.1 g of catalyst (anode or cathode powder with ∼80 mesh grain size) was put in the center of the reactor, and a K-type thermocouple was immersed into the catalyst bed with the protection of a small quartz tube to avoid catalytic contribution to the methane conversion. A tube furnace was applied to sustain the temperature required for the reaction. Methane–air mixed gas was introduced from the top of the reactor. The effluent gas from the bottom of the reactor was introduced to a Varian 3800 gas chromatograph, which was equipped with a Poraplot Q and 5 Å molecular sieve capillary columns for the separation of $H_2$, $O_2$, CO, $CO_2$ and $CH_4$. Before introduction into the reactor, water was adsorbed by a cooling trap. The methane and oxygen conversions were calculated based on

$$\%\ \text{conversion}_{CH_4} = \frac{[CO] + [CO_2]}{[CO] + [CO_2] + [CH_4]_{\text{outlet}}} 100$$

$$\%\ \text{conversion}_{O_2} = \frac{(1/2)[CO] + [CO_2] + (1/2)[H_2O]}{(1/2)[CO] + [CO_2] + (1/2)[H_2O] + [O_2]_{\text{outlet}}} 100$$

And the CO and $CO_2$ selectivity was calculated based on

$$\%\ \text{selectivity}_{CO_2} = \frac{[CO_2]}{[CO + CO_2]} 100$$

$$\%\ \text{selectivity}_{CO} = \frac{[CO]}{[CO] + [CO_2]} 100$$

### 2.4. Characterization

X-ray diffractometer (XRD, Bruker D8 Advance) was used to analyze chemical compatibilities against high temperature and stability against reducing atmosphere. The microscopic features and element compositions of the electrodes were characterized using an environmental scanning electron microscope (ESEM, QUANTA-2000) equipped with an energy dispersive X-ray (EDX) attachment. The electrode performance was investigated with complete cell configuration by the ac impedance method using an electrochemical workstation based on the Solartron 1287 potentiostat in combination with a Solartron 1260A frequency response analyzer. The frequency range applied was from 0.01 Hz to 100 kHz with signal amplitude of 10 mV under OCV conditions. The overall impedance data were fitted by a complex nonlinear least squares (CNLSs) fitting program in Z-View 2.9b software.

## 3. Results and discussion

### 3.1. Initialization by methane and air mixed gas

Because the SC-SOFC in this study operates on a methane–air mixture, the most practical approach to fuel cell initialization is the through the application of the same mixed gas or through using pure methane as the reduction gas. Shao et al. have demonstrated that the highest performance for a SC-SOFC with similar cell components to those in this study was achieved at the methane to oxygen ratio of ∼1:1 [28]. Therefore a methane–air mixture with the same methane to oxygen ratio was investigated in this study for the initialization of the fuel cell at 800 °C (methane to air ratio of 90:380). During the initialization process the OCV of the fuel cell was in situ monitored. Once the anode was successfully reduced, the resulting nickel metal would catalyze the partial oxidation of methane to syngas and then create a significant decrease in the oxygen partial pressure over the anode surface. Consequently, a large OCV should be observed due to the large oxygen potential difference between the anode and cathode surfaces. As shown in Fig. 2, a steady increase of the OCV was observed over time. However, the cell voltage increased very slowly from an initial value

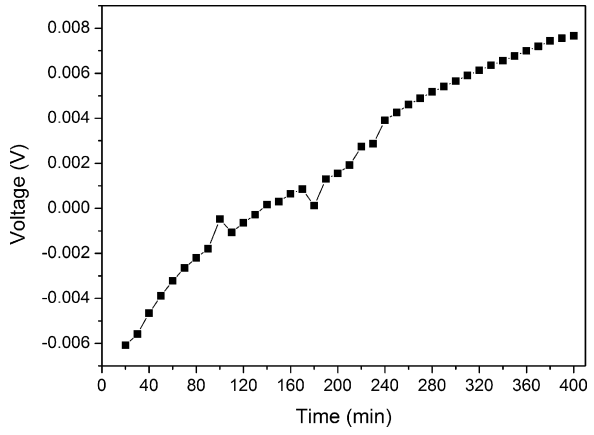


Fig. 2. The time-dependence of the cell OCV during the initialization process with methane and air mixed gas as the reduction gas.

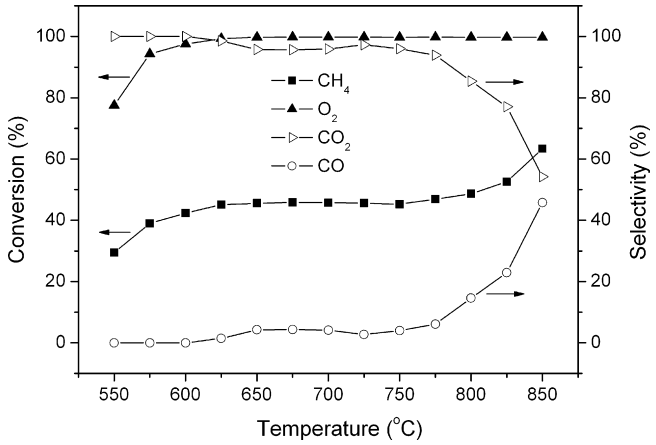


Fig. 4. Methane and $O_2$ conversions, CO and $CO_2$ selectivity of NiO + SDC catalysts for methane oxidation at various temperatures between 550 and 850 °C.

of −0.006–0.007 V after about 6.5 h on stream. This suggests that the initialization was actually unsuccessful. After the treatment, the fuel cell maintained perfect geometric integrity with no carbon deposition detected over both the cathode and anode surfaces. The room-temperature conductivity was so low that it was out of the range of the multimeter. XRD patterns of the anode, before and after the treatment of the fuel cell by $CH_4$ + air mixed gas, are shown in Fig. 3. It can be seen that the nickel in the anode still took the oxidation state of NiO after the treatment.

Whether or not the anode can be successfully activated by the methane–air mixed gas during the in situ initialization process is closely related to the catalytic activity of the NiO + SDC anode towards the gas mixture. Fig. 4 shows the temperature dependence of methane/oxygen conversions and $CO/CO_2$ selectivity over the unreduced NiO + SDC anode catalyst between 550 and 850 °C. It was observed that NiO + SDC had medium catalytic activity for methane deep oxidation to $CO_2$ and $H_2O$. At 800 °C, the oxygen and methane conversions reached ∼99.8 and ∼50%, respectively. The chemical stability of NiO and Ni depends on both the temperature and the partial pressure of oxygen in the atmosphere. The equilibrium oxygen partial pressure for the reaction $NiO \leftrightarrow Ni + 1/2O_2$ (g) is around $9.1 \times 10^{-10}$ atm at 800 °C [31]. This means that thermodynamically nickel oxide can be reduced to Ni metal only at $P_{O_2} < 9.1 \times 10^{-10}$ atm at 800 °C. The actual oxygen partial pressure over the NiO + SDC surface, which was calculated based on the unreacted oxygen, reached $\sim 10^{-5}$ atm. Such high oxygen partial pressure, which was previously related to the poor activity of NiO + SDC for oxygen conversion, accounts for the unsuccessful activation of the anode, i.e., the reduction of NiO to Ni, by applying the methane–air mixture as the reduction gas.

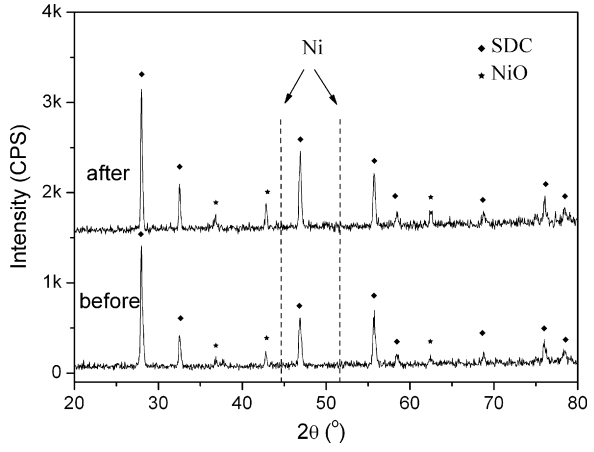


Fig. 3. XRD patterns of the anode before and after the pre-treatment with methane and air mixed gas.

### 3.2. In situ reduction of anode by pure methane

Considering the high oxygen partial pressure of the anode atmosphere by applying methane–air mixture as the initialization gas, pure methane, a more reducing gas, was investigated for in situ reduction of SC-SOFC anode. After the fuel cell was treated with methane at 800 °C for ∼400 min, the methane–air mixed gas was turned on and the time dependence of OCV was recorded. Near zero OCV was also observed. This suggests that the initialization of the fuel cell by pure methane also failed. Electrochemical impedance spectroscopy (EIS) measurements demonstrate that the fuel cell had an area specific bulk resistance of less than 0.6 Ω $cm^2$ at 800 °. Therefore, the anode was actually successfully reduced after the methane treatment. However, the fuel cell was badly distorted and swelled significantly with a cell diameter increase of more than 40%. Shown in Fig. 5 are the XRD patterns of the anode after the in situ reduction by methane. Only metal nickel and SDC phases were detected, which further supports that the successful reduction of the anode was achieved.

The surface morphologies of the anode and cathode before and after the methane treatment were examined by SEM. When compared to the fresh anode (Fig. 6A), it could be seen that the porosity of the anode after the treatment was significantly increased (Fig. 6B). On the other hand, large amounts of carbon fibers were observed inside the anode layer. Their formation was closely related to the high catalytic activity of nickel for methane cracking [32,33]. Significant carbon formation was supported by

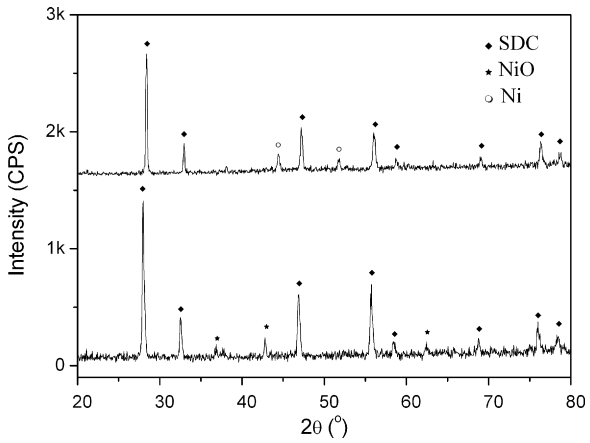


Fig. 5. X-ray diffraction patterns of the anode before and after the in situ reduction by pure methane.

the EDX detection as shown in Fig. 6C. Although the EDX is not a perfect tool for the detection of carbon contents due to the easy carbon contamination during the sample preparation process, especially for quantitatively determination of the carbon content. However, through careful management, it can still be applicable to determine carbon qualitatively. During the sample preparation, we take care to avoid the carbon contamination to the maximum degree. Furthermore we conducted the EDX examination for the hydrogen reduced sample in parallel. The EDX result of the hydrogen-reduced sample showed only weak carbon peak (Fig. 6D). It suggests that the carbon contamination during the sample preparation is small. As compared to the hydrogen reduced anode, the carbon peak of the methane reduced anode is in much higher intensity (more than 200 times in peak height). Since they were prepared in parallel for the EDX examination, the carbon from the source of contamination should be comparable for the two samples. Therefore, the carbon peak in the EDX profile of the methane reduced anode is mainly contributed from the formed carbon, instead of contamination. The carbon coking resulted in severe cell distortion and expansion as well as the detachment of the cathode from electrolyte surface. Fig. 7A and B is the SEM photos of the cathode before and after the methane treatment. No carbon coking was observed over the cathode layer after the methane treatment. However, its grain size reduced significantly when compared to the new cathode. The significant distortion of the fuel cell and the detachment of the cathode from the electrolyte then accounts for the failure of the fuel cell's initialization with methane as the reducing agent.

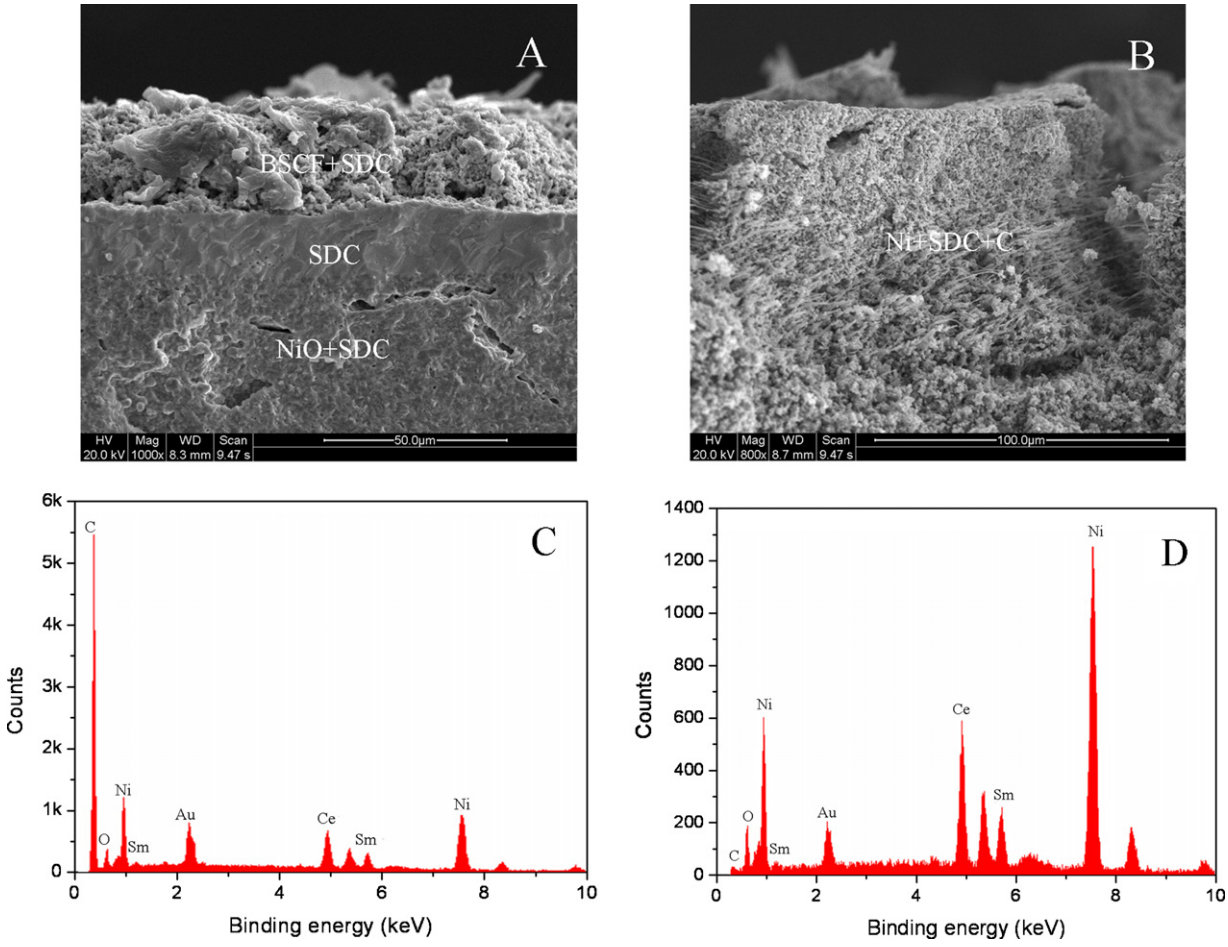


Fig. 6. (A and B) Cross sectional SEM micrographs of the anode (A) before initialization by methane and (B) after the initialization by methane; the EDX profiles of (C) the methane activated anode and (D) the hydrogen reduced anode (cross section).

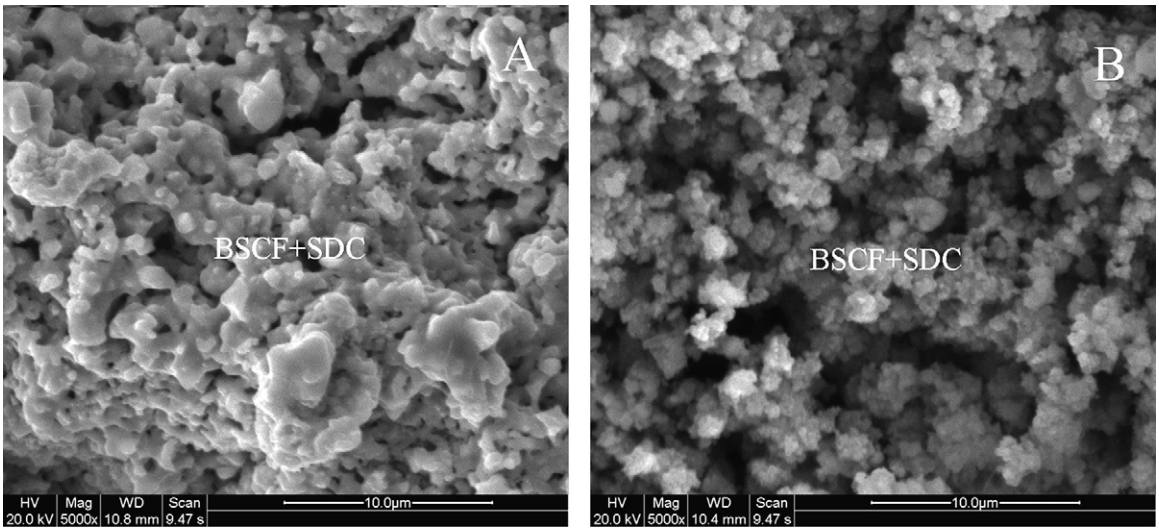


Fig. 7. The surface morphologies of the cathode (A) before and (B) after the methane treatment.

### 3.3. In situ reduction with hydrogen

In order to prevent carbon coking over the anode by applying methane as the reduction gas for the fuel cell initialization, the in situ reduction of the anode by hydrogen was then tried. Once the fuel cell temperature reached 600 °C under nitrogen atmosphere, the atmosphere was switched to hydrogen with its flow direction parallel to the electrode surfaces. After the fuel cell temperature was dwelled at 600 °C under the hydrogen atmosphere for 30 min, the methane–air mixture was the turned on and an instant response of the OCV was recorded. As shown in Fig. 8, the fuel cell envisaged a sharp increase of the OCV to around 0.6 V within the first 15 min, and then slowly increased to ~0.7 V after an equilibrium time of about 50 min. This suggests that the in situ reduction of the anode in a single-chamber configuration might be practically feasible.

Fig. 9 shows the steady state *I–V* curves of the fuel cell at a furnace temperature of 575–700 °C after initialized by in situ hydrogen reduction. Within the investigated furnace temperature range of 575–700 °C, it was observed that higher operation temperatures resulted in lower OCV. The fuel cell delivered a promising power density of ~325 mW cm$^{-2}$ at a furnace temperature of 575 °C and ~350 mW cm$^{-2}$ at 600 °C. The typical EIS is shown in Fig. 10. The fuel cell shows a relatively low electrode polarization resistance of ~0.21 Ω cm$^2$, which is about the same as the electrolyte ohmic drop. No substantial difference in the EIS was observed between different furnace temperatures.

The in situ reduction of the anode by hydrogen fuel is the most frequently applied technique for the initialization of a dual-chamber SOFC. Since the anode atmosphere does not reach the cathode in a dual-chamber configuration, the anode reaction typically has no impact on the cathode stability. In the single-chamber configuration, the spontaneous reduction of the cathode by hydrogen could also occur during the anode reduction, since the hydrogen stream sweeps not only the anode but also the cathode. BSCF is intrinsically unstable under hydrogen atmosphere, which was reduced to Co, Fe and BaO/Ba(OH)$_2$.$x$H$_2$O, SrO/(Sr(OH)$_2$.$x$H$_2$O [34]. Fig. 11 shows the XRD diffraction of both anode and cathode after treatment in the hydrogen atmosphere at 600 °C for 30 min. This demonstrated that the anode

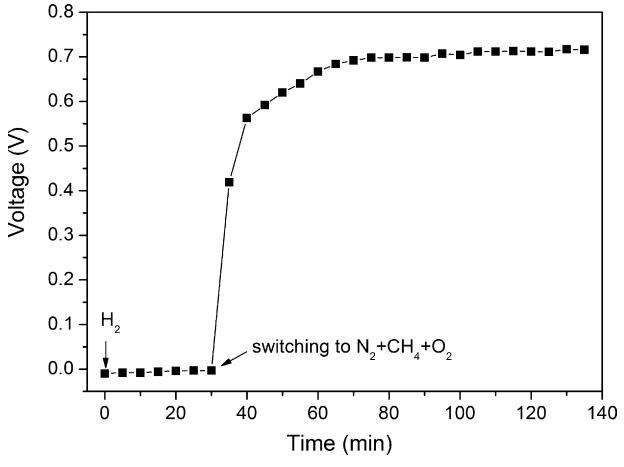


Fig. 8. The time-dependence of the cell OCV as in situ reduced by hydrogen.

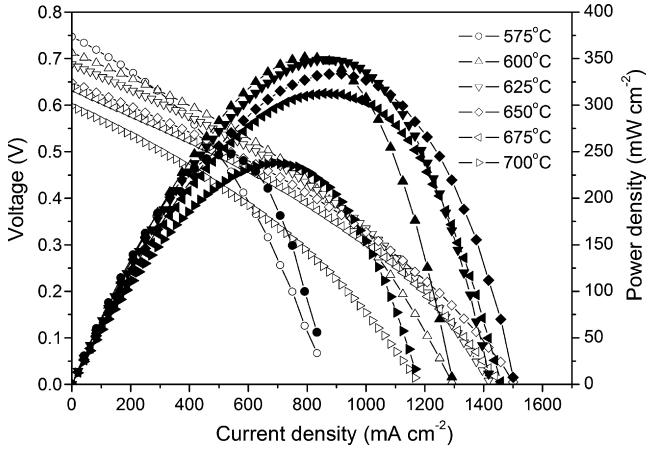


Fig. 9. *I–V* and *P–I* curves of the NiO + SDC|SDC|BSCF + SDC fuel cells initialized by in situ hydrogen reduction.

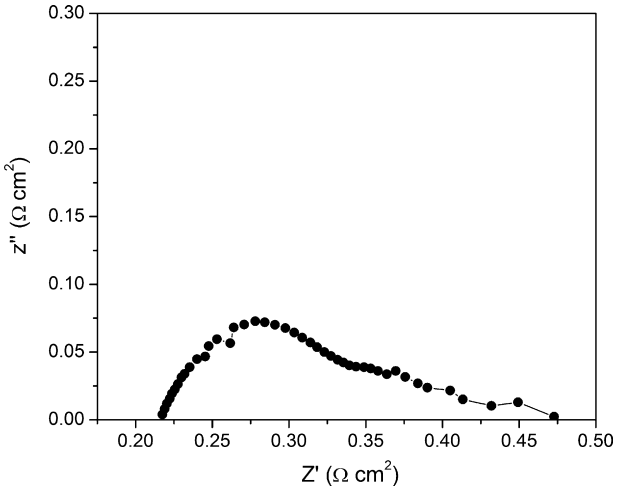


Fig. 10. Typical impedance spectroscopy of the fuel cell initialized by in situ hydrogen reduction measured at furnace temperature of 575 °C.

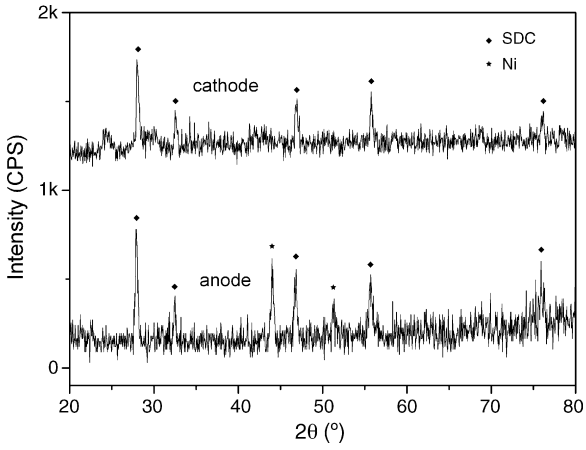


Fig. 11. X-ray diffraction patterns of the anode and cathode after the in situ hydrogen reduction at 600 °C for 30 min.

was successfully reduced to metal nickel, while the BSCF perovskite phase in the cathode was totally destroyed. The reduction and decomposition products of BSCF formed an amorphous phase.

Since cobalt is typically a good catalyst for methane partial oxidation [35,36], the acquirement of high OCV and power density was somewhat surprising. Fig. 12 shows the catalytic activity of fresh and reduced BSCF towards methane conversion. It is very interesting that the reduced BSCF also showed very poor activity, similar to the fresh BSCF, for the methane deep oxidation and partial oxidation. It is suspected that the iron and BaO/SrO, $Ba(OH)_2.xH_2O/Sr(OH)_2.xH_2O$ phases may reduce the catalytic activity of cobalt for methane partial oxidation. The poor activity resulted in high oxygen partial pressure over the cathode, while the partial oxidation of methane created a highly reducing atmosphere over the reduced anode surface, and consequently a high OCV was observed.

It was reported that BSCF has very good phase reversibility capacity. Once the oxidant atmosphere (such as oxygen) can be restored in time, the reduced BSCF could restore its perovskite phase structure under an air atmosphere at high temperatures. Such a unique property was believed to be the cause for the stable operation of the BSCF reactor for the partial oxidation of methane to syngas, in which a highly reducing environment is usually expected at the reaction side [34]. It is likely that the high cathode performance of the in situ activated fuel cell with hydrogen is also closely related with the high phase reversibility of the BSCF oxide. To support this assumption, a pre-reduction/re-oxidation under air + $CH_4$ atmosphere experiment was conducted. Fig. 13 shows the XRD patterns of the reduced-BSCF oxide after being treated at 800 °C for various times under a methane–air atmosphere. Thus, the reduced BSCF restored its main peorvskite structure after re-treatment in methane–air atmosphere for 80 min.

### 3.4. Pre-reduction of the anode by hydrogen before cathode deposition

The most ideal initialization process should result in the complete reduction of the anode while not influencing the cathode. Since the anode and cathode are exposed in the same gas cham-

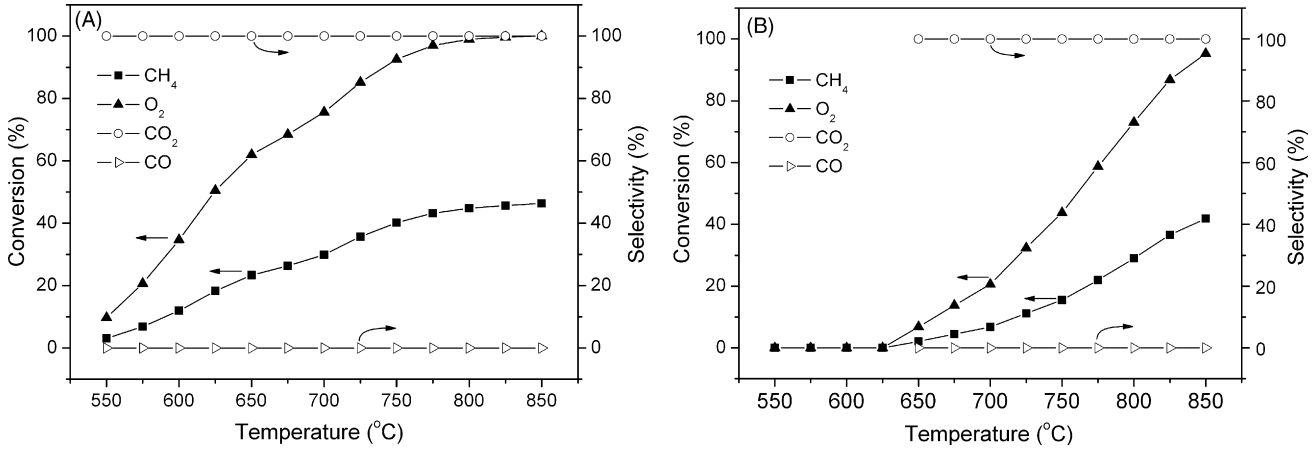


Fig. 12. Methane and $O_2$ conversions, CO and $CO_2$ selectivity over (A) fresh, and (B) reduced BSCF + SDC catalysts at various temperatures between 550 and 850 °C.

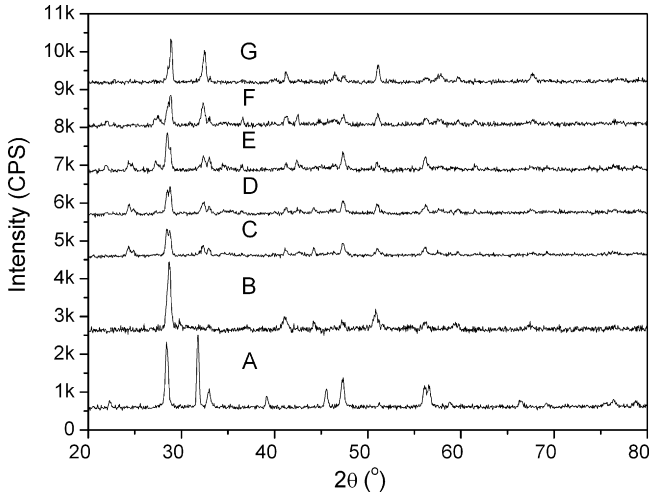


Fig. 13. X-ray diffraction patterns of BSCF + SDC powder (A) fresh, (B) reduced 30 min by $H_2$ at 600 °C, (C), (D), (E), (F) and (G) treated under a methane–air atmosphere for 5, 20, 40, 60 and 80 min, respectively.

ber, the reduction of the cathode would be unavoidable during the in situ initialization of the fuel cell by hydrogen. An ex situ reduction of the anode was then tried. The anode-supported thin-film electrolyte dual layer was pre-reduced by hydrogen, after the deposition of the cathode layer; the complete cell was fired at 1000 °C under a nitrogen atmosphere to prevent the re-oxidation of the anode. Through the above process, the reduced state of the nickel in the anode and the perovskite structure of the BSCF in the cathode were ensured.

The fuel cell was first heated in nitrogen. Once it reached 600 °C, the mixed methane–air gas was turned on. A quick response of the OCV was observed, suggesting that the partial oxidation over the anode was initialized and stabilized very fast due to being catalyzed by the reduced anode. The fuel cell quickly reached an OCV of ~0.75 V, then decreased slightly with time on stream, and finally remained at a steady value of ~0.73 V after about 5 min of equilibrium time. The fuel cell performance also improved slightly with time on stream, from an initial peak power density of ~500 mW $cm^{-2}$ to a steady value of 570 mW $cm^{-2}$. Both the increment in fuel cell performance and the decline in OCV were attributed to the elevation of the actual fuel cell temperature due to the partial oxidation/combustion over the anode surface. The oxidation of methane over the fuel cell anode is exothermal in nature, which could result in a fuel cell temperature ten to hundreds degrees higher than the furnace temperature [37,38]. Such an increase not only decreased the electrolyte ohmic resistance but also accelerated the electrode kinetics, which is beneficial for improving the fuel cell performance. However, the elevated temperature also enhanced the non-electrochemical oxidation of methane over the cathode and resulted in a decrease of the OCV. The gas-phase combustion also accounts in part to the decrease of OCV with temperature.

Fig. 14 shows *I–V* curves of the fuel cells operated at various furnace temperatures. The maximum peak power density of 570 mW $cm^{-2}$ was achieved at a furnace temperature between 575 and 700 °C. It was much higher than that observed for the fuel cell with the in situ reduced anode by hydrogen at similar

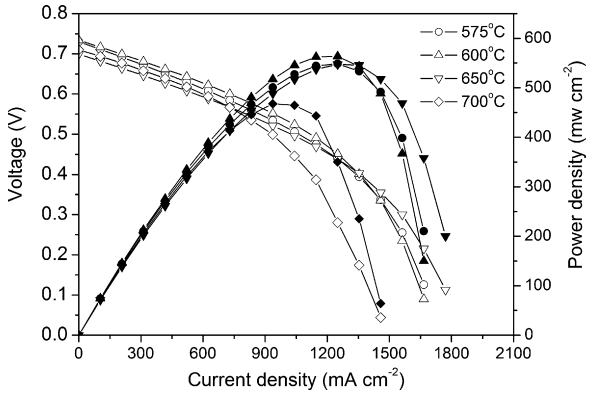


Fig. 14. *I–V* and *P–I* curves of the NiO + SDC|SDC|BSCF + SDC fuel cells at various temperature between 575 and 700 °C furnace temperatures initialized by ex situ hydrogen reduction.

operational conditions (350 mW $cm^{-2}$). The impedance spectroscopes of the fuel cell were also examined under an OCV condition with the typical EIS shown in Fig. 15. The fuel cell demonstrates an overwhelming polarization resistance from the electrolyte, which is about three times that of the electrode polarization resistance, including both the anode and cathode.

As compared to the OCV of a dual-chamber fuel cell using YSZ electrolyte and syngas as fuel (~1.15 V), the OCV in this study is relatively low, which is mainly contributed from two aspects. Firstly, SDC will not perform as a pure oxygen ionic conductor at the fuel cell operation condition of this study. Since the fuel cell temperature in single-chamber configuration could be several tens to hundreds degree higher than the furnace temperature, the real fuel cell temperature is around 700–800 °C in this study. At such high temperature, the electronic conductivity of SDC electrolyte is not negligible, which caused internal current short and resulted in lowering OCV. Secondly, the non-ideal performance of anode and cathode towards methane–air mixture caused mixed potential over the electrodes, which then led to additional decrease of the open circuit voltage.

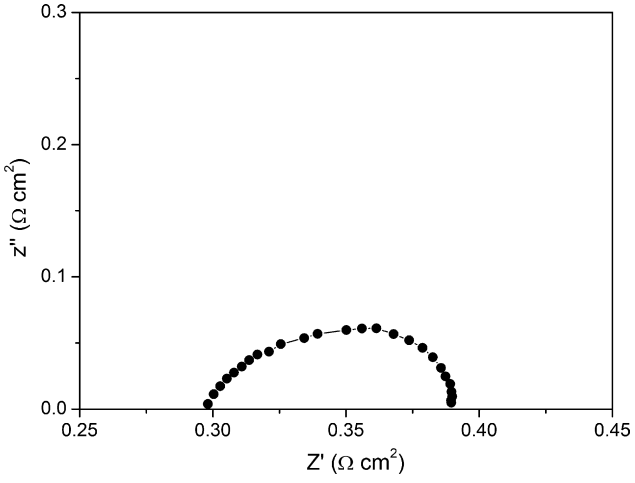


Fig. 15. Typical impedance spectroscopy of the fuel cell initialized by ex situ hydrogen reduction, measured at a furnace temperature of 575 °C.

## 4. Conclusions

The performance of the anode-supported SC-SOFC based on a NiO + SDC anode and BSCF + SDC cathode are strongly related to the initialization process. Methane–air mixed gas failed to reduce NiO due to the poor activity of NiO towards methane oxidation. Although successful reduction of NiO was achieved by applying pure methane as the initialization gas, the anode experienced severe carbon deposition, which resulted in the severe distortion of the fuel cell, and consequently zero power was generated from this fuel cell. The initialization of the NiO anode SC-SOFC by in situ reduction with hydrogen was somewhat successful. A peak power density of ~325 and 350 mW cm$^{-2}$ was achieved at a furnace temperature of 575 and 600 °C, respectively, which was closely related to the high phase reversibility of BSCF. The pre-reduction of the anode by hydrogen before cathode deposition was found to be a more suitable method of initialization. With this method, the BSCF can maintain perfect perovskite structure during the anode reduction, which then ensures the high performance of the fuel cell. Under optimized conditions, a peak power density as high as 550–570 mW cm$^{-2}$ was observed at a furnace temperature of 575–600 °C with a methane–air stream for both the anode and cathode. EIS examination suggests that the electrolyte ohmic drop was the overwhelming resistance for the fuel cell. A decrease of electrolyte thickness would further increase the fuel cell performance. Based on above analysis, it is clear that the reduction of the anode before the cathode deposition is the most suitable method for the initialization of the fuel cell with a Ni + SDC anode and BSCF + SDC cathode operated in a single-chamber configuration with methane–air mixture.

## Acknowledgements

This work was supported by the National Natural Science Foundation of China under contract, Nos. 20646002 and 20676061, and National Basic Research Program of China under contract No. 2007CB209704.

## References

[1] C.K. Dyer, Nature 343 (1990) 547–548.
[2] B.C.H. Steele, A. Heinzel, Nature 414 (2001) 345–352.
[3] Y. Inui, A. Urata, N. Ito, T. Nakajima, T. Tanaka, Energy Convers. Manage. 47 (2006) 1738–1747.
[4] S.W. Zha, A. Moore, H. Abernathy, M.L. Liu, J. Electrochem. Soc. 151 (2004) A1128–A1133.
[5] K. Sasaki, K. Watanabe, Y. Teraoka, J. Electrochem. Soc. 151 (2004) A965–A970.
[6] T. Hibino, A. Hashimoto, T. Inoue, J. Tokuno, S. Yoshida, M. Sano, Science 288 (2000) 2031–2033.
[7] Z.P. Shao, C. Kwak, S.M. Haile, Solid State Ionics 175 (2004) 39–46.
[8] T.W. Napporn, X. Jacques-Bedard, F. Morin, M. Meunier, J. Electrochem. Soc. 151 (2004) A2088–A2094.
[9] B.E. Buergler, M.E. Siegrist, L.J. Gauckler, Solid State Ionics 176 (2005) 1717–1722.
[10] T. Suzuki, P. Jasinski, V. Petrovsky, H.U. Anderson, F. Dogan, J. Electrochem. Soc. 152 (2005) A527–A531.
[11] M. Kuhn, T. Napporn, M. Meunier, D. Therriault, S. Vengallatore, Mater. Res. Soc. Symp. Proc. 972 (2007) 211–216.
[12] M.L. Liu, Z. Lü, B. Wei, R.B. Zhu, X.Q. Huang, K.F. Chen, G. Ai, W.H. Su, J. Electrochem. Soc. 154 (2007) B588–B592.
[13] T. Hibino, A. Hashimoto, M. Suzuki, M. Yano, S. Yoshida, M. Sano, J. Electrochem. Soc. 149 (2002) A195–A200.
[14] D. Rotureau, J.P. Viricelle, C. Pijolat, N. Caillol, M. Pijolat, J. Eur. Ceram. Soc. 25 (2005) 2633–2636.
[15] I. Riess, P.J. van der Put, J. Schoonman, Solid Stale Ionics 82 (1995) 1–4.
[16] M. Yano, A. Tomita, M. Sano, T. Hibino, Solid State Ionics 177 (2007) 3351–3359.
[17] B.E. Buergler, A.N. Grundy, L.J. Gauckler, J. Electrochem. Soc. 153 (2006) A1378–A1385.
[18] T. Suzuki, P. Jasinski, V. Petrovsky, H.U. Anderson, F. Dogan, J. Electrochem. Soc. 151 (2004) A1473–A1476.
[19] T. Hibino, A. Hashimoto, M. Yano, M. Suzuki, S. Yoshida, M. Sano, J. Electrochem. Soc. 149 (2002) A133–A136.
[20] B. Morel, R. Roberge, S. Savoie, T.W. Napporn, M. Meunier, Appl. Catal. A: Gen. 323 (2007) 181–187.
[21] X. Jacques-Bedard, T.W. Napporn, R. Roberge, M. Meunier, J. Power Sources 153 (2006) 108–113.
[22] I. Riess, C.G. Vayenas, Solid State Ionics 159 (2003) 313–329.
[23] T. Hibino, S.Q. Wang, S. Kakimoto, M. Sano, Electrochem. Solid State Lett. 2 (1999) 317–319.
[24] A.K. Demin, F.Y. Gulbis, Solid State Ionics 135 (2000) 451–456.
[25] Y. Hao, Z.P. Shao, J. Mederos, W. Lai, D.G. Goodwin, S.M. Haile, Solid State Ionics 177 (2006) 2013–2021.
[26] Z.P. Shao, S.M. Haile, Nature 431 (2004) 170–173.
[27] Z.P. Shao, S.M. Haile, J. Ahn, P.D. Ronney, Z.L. Zhan, S.A. Barnett, Nature 435 (2005) 795–798.
[28] Z.P. Shao, J. Mederos, W.C. Chueh, S.M. Haile, J. Power Sources 162 (2006) 589–596.
[29] W. Zhou, Z.P. Shao, W.Q. Jin, J. Alloys Compd. 426 (2006) 368–374.
[30] H.X. Gu, R. Ran, W. Zhou, Z.P. Shao, J. Power Sources 172 (2007) 704–712.
[31] M.X. Jing, X.Q. Shen, Y.J. Shen, J. Inorg. Mater. 19 (2004) 289–294.
[32] R. Aiello, J.E. Fiscus, H. zur Loye, M.D. Amiridis, Appl. Catal. A: Gen. 192 (2000) 227–234.
[33] S. Fukada, N. Nakamura, J. Monden, M. Nishikawa, J. Nucl. Mater. 329–333 (2004) 1365–1369.
[34] Z.P. Shao, W.S. Yang, Y. Cong, H. Dong, J.H. Tong, G.X. Xiong, J. Membr. Sci. 172 (2000) 177–188.
[35] X.L. Zhang, C.S.M. Lee, D.M.P. Mingos1, D.O. Hayward, Appl. Catal. A: Gen. 248 (2003) 129–142.
[36] R. Lødeng, E. Bjørgum, B.C. Enger, J.L. Eilertsen, A. Holmen, B. Krogh, M. Rønnekleiv, E. Rytter, Appl. Catal. A: Gen. 333 (2007) 11–23.
[37] T. Hibino, A. Hashimoto, T. Inoue, J. Tokuno, S. Yoshida, M. Sano, J. Electrochem. Soc. 148 (2001) A544–A549.
[38] T.W. Napporn, F. Morin, M. Meunier, Electrochem. Solid State Lett. 7 (2004) A60–A62.